Interactions in bisamide ionic liquids—insights from a Hirshfeld surface analysis of their crystalline states†

Pamela M. Dean,* Jennifer M. Pringle, Craig M. Forsyth, Janet L. Scott and Douglas R. MacFarlane

Received (in Montpellier, France) 6th June 2008, Accepted 25th July 2008
First published as an Advance Article on the web 9th September 2008
DOI: 10.1039/b809606f

The intermolecular interactions of a series of crystallised bis(trifluoromethanesulfonyl)amide (NTf_2) and bis(methanesulfonyl)amide ($NMes_2$) ionic liquids are qualitatively investigated and compared using Hirshfeld surface and thermal analysis techniques. The $NMes_2$ salts are known to exhibit higher glass transitions and higher viscosities than those of the NTf_2 salts. The origins of these differences were analysed in terms of the importance of factors such as the C–H···O hydrogen bond, fluorination, presence of an aromatic moiety and length of alkyl chain, using the Hirshfeld surfaces and their associated fingerprint plots. Additionally, the existence of C–F···π and C–H···π interactions were elucidated and the significance of anion–anion interactions was recognised. Overall, these results demonstrate the applicability of the Hirshfeld surface approach in investigating the molecular origins of the physical properties.

Introduction

Ionic liquids (ILs) are becoming important alternatives for a variety of applications such as non-volatile solvents and extractants in chemical synthesis,[1–3] highly stable electrolytes in electrochemical devices[4] and as active pharmaceutical ingredients.[5] It has become apparent that one of the IL anions of choice in terms of high thermal, chemical and electrochemical stability is the bis(trifluoromethanesulfonyl)amide (NTf_2) ion. The first ionic liquids comprising the NTf_2 anion were used as solventless electrolytes within electrochemical devices, where the anion was specifically designed for its thermochemical and electrochemical stability.[6,7] It was reasoned that the perfluorinated anion displayed a lower Lewis basicity than the traditionally used $AlCl_4^-$ anion, thus rendering them chemically benign. In addition, the anion displays a delocalisation of the negative charge, thus reducing the likelihood of hydrogen bonding and ultimately lowering the viscosity–both favourable aspects of an anion for an electrolyte.[6,8]

Subsequently, analogues of the NTf_2 anion, such as bis(methanesulfonyl)amide ($NMes_2$), were designed to produce room-temperature ionic liquids combined with the *N*-alkyl-1-methylpyrrolidinium ($C_x$mpyr) and the *N*-alkyl-3-methylimidazolium ($C_x$mim) cations. It was reasoned that the analogous $NMes_2$ ILs would be usefully hydrophilic and lower melting, however, the ILs were also found to display decreased thermal and electrochemical stability and increased viscosity, thus rendering them less useful for electrochemical devices.[9]

Several articles have appeared detailing the structural analysis of cryo-crystallised NTf_2 ionic liquids, with the intention of understanding the physical properties of the liquid state.[10–14] Apart from recognition of the anion *cis*/*trans* conformation and packing, much attention has been placed on the existence of C–H···O type hydrogen bonding between the cation and anion. It has been concluded in some reports that this inter-ionic hydrogen bonding, along with other weak intermolecular interactions, contributes to the stability of the resultant crystalline state.[9,12–14] In order to further investigate these important interactions, the need arises to consolidate information and compare the reported crystal structures with the aim of quantifying the similarities and differences. Hirshfeld surfaces have been found to be a powerful tool in the examination of intermolecular interactions when a crystal structure is available (further details on the Hirshfeld surface are provided below).[15–18] Notably, a two-dimensional grid called a 'fingerprint plot' can be constructed from the corresponding three-dimensional Hirshfeld surface. Essentially the fingerprint plot, which charts the distance to the nearest atom external to the Hirshfeld surface (d_e) against the distance to the nearest atom internal to the surface (d_i), is a condensed informative map of all the intermolecular interactions occuring in the crystal. In addition, the plots can be decomposed to provide the relative contributions of each intermolecular interaction. Both facilities leads to a practical, concise summary of all the essential structural information required for rapid comparison of structures.

Thus, in this work a selection of NTf_2 and $NMes_2$, *N*-alkyl-1-methylpyrrolidinium ($C_x$mpyr) and *N*-alkyl-3-methylimidazolium ($C_x$mim) salts have been chosen in order to obtain a comparative understanding of the role of the intermolecular

Department of Chemistry, Monash University, Wellington Road, Clayton, Victoria, 3800, Australia.
E-mail: pamela.dean@sci.monash.edu.au; Fax: +61 3 9905 4597; Tel: +61 3 9905 4599

† Electronic supplementary information (ESI) available: Additional detailed crystallographic, analysis and analysis of fingerprint plots of all compounds and the crystallographic information files. CCDC reference numbers 701482 and 701483. For ESI and crystallographic data in CIF or other electronic format see DOI: 10.1039/b809606f

interactions present, in particular the importance of the C–H···O hydrogen bond, fluorination, presence of an aromatic moiety and length of alkyl chain. To this end we report, for the first time, crystal structures for $[C_4mpyr][NMes_2]$ and $[C_2mim][NMes_2]$. These along with known structures of $[C_1mpyr][NMes_2]$[9] (CSD refcode: ULOJOU), $[C_1mpyr][NTf_2]$[10] (CSD refcode XOMDIM), $[C_4mpyr][NTf_2]$[12] (CSD refcode LAZREK), and $[C_2mim][NTf_2]$[13] (CSD refcode RENSEJ) allow a comprehensive comparison of the structures *via* the Hirshfeld surface analysis.

Results and discussion

Thermal analysis

Crystallisation of $[C_4mpyr][NMes_2]$ and $[C_2mim][NMes_2]$ was observed in the neat ionic liquids after careful storage of the original samples for >2 years.[9] Crystal structures were obtained from these samples (see ESI†) and are compared to the structures of crystallised NTf_2 analogues already published.[9,10,12,13] DSC analysis of the $NMes_2$ crystals melted in the DSC show the same glass transition temperatures (T_g) as those originally reported (Table 1).[9] All T_gs are approximately 30 °C higher than those measured for the NTf_2 salts. In addition, within the NTf_2 series, the glass transition temperature increases with increasing alkyl chain length whereas there is little change in the $NMes_2$ case.

Hirshfeld surface and fingerprint plot generation

A Hirshfeld surface analysis of each of the crystal structures (detailed comparative X-ray analysis are also provided in the ESI†) has been carried out, producing the Hirshfeld surface for each ion in each structure, for example that shown in Fig. 1 for the $NMes_2$ anion in $[C_2mim][NMes_2]$. The Hirshfeld surface can be defined as 'the portion of space where the *promolecule* electron density contributes more than half of the total *procrystal* electron density'.[17] The surface is defined so that for each point on the surface "1/2 of the electron density is due to the spherically averaged non-interacting atoms comprising the molecule, and the other half is due to those comprising the rest of the crystal".[17] So, the surface is "a region of space surrounding a particular molecule in a crystal where the electron distribution of that molecule exceeds that due to any other molecule".[17] Close contacts can then be shown on this surface by calculating a normalised contact distance, d_{norm}, which compares the distance between two atoms across the surface to the combined van der Waal radii of the atoms.[18] A colour scheme is applied such that where the contact is shorter than the van der Waals separation the point is coloured red, white is used for contacts around the van der Waals separation and blue is for longer contacts. The Hirshfeld surface can then be thought of as an "interaction surface" that highlights and identifies important interactions in the crystal. Hirshfeld surfaces and their associated fingerprint plots were generated using the program *CrystalExplorer*.[15]

The fingerprint plot plots the distance (d_i) from the nearest atom inside the surface against the distance (d_e) to the nearest atom external to the surface, as shown in Fig. 1 for the C_2mim $NMes_2$ case; the fingerprint plots for all of the other salts are presented in the ESI.† The fingerprint plot provides information on the fraction of the Hirshfeld surface area due to any particular contact and how extensive that fraction is in distance. The colour coding in the fingerprint plot represents the frequency of occurrence of any given (d_i, d_e) pair with white = no occurrence, blue = some occurrence, and green then red indicating more frequent occurrence. For further detailed analysis, *Crystal Explorer* also allows the isolation of any given interaction (*e.g.*: C–H···O) and then the generation of a 'decomposed' fingerprint plot, where only the relevant interactions are coloured, and the associated Hirshfeld surface coloured for that interaction alone;[18] see for example Fig. 2 which isolates the CH···O interactions in $[C_2mim][NMes_2]$. Similarly, decomposed fingerprint plots for the other interactions are presented in the ESI.† As part of this decomposition analysis, the fraction of the surface representing a given interaction was also calculated (see for example Table 2). It is important to note that each close contact in the crystal structure generates many points in the fingerprint plot (*i.e.* many (d_i, d_e) pairs arising from the close contact).

In the prior literature, the important intermolecular interactions identified as likely to be of significance in $[C_1mpyr][NTf_2]$[10] were the inter-ionic C–H···O and C–H···N hydrogen bonds and the weaker non-classical C–H···F hydrogen bonds. Those identified in $[C_4mpyr][NTf_2]$[12] were the inter-ionic C–H···O hydrogen bonds, and in $[C_2mim][NTf_2]$[13] the C–H···O hydrogen bond and C–F···F interactions. All of these interactions are clearly seen in the Hirshfeld analysis of the structures (as presented in the ESI†) which also provides information as to their relative contributions to the whole "interaction surface", as listed in Table 2 and Table 3. The $[C_2mim][NTf_2]$ case is an interesting example where the crystal structure contains two crystallographically distinct anions and cations and the analysis allows the straightforward identification of their individual interactions as shown in Table 2 and Table 3.

The Hirshfeld analysis also reveals the additional occurrence of inter-*anionic* interactions in these compounds. Table 3 lists selected interactions and their relative contributions in each case.

The trend seen from the percentage contributions is that the $NMes_2$ salts have a larger contribution from the C–H···O and C–H···N inter-ionic contacts, to the entire Hirshfeld surface area, which could contribute to an increased lattice energy over that of the NTf_2 salts. Obviously, with increasing alkyl chain length in both salts the C–H···X contribution increases. The decomposition of the anionic interactions clearly indicates the occurrence of contacts between the anions and that there is

Table 1 Comparison of the glass transition temperatures of the $NMes_2$ and NTf_2 ionic liquids[9]

	$NMes_2$ T_g/°C	NTf_2 T_g/°C
$[C_1mpyr]$	−58	—
$[C_2mpyr]$	−64	−102
$[C_3mpyr]$	−63	−90
$[C_4mpyr]$	−58	−87
$[C_2mim]$	−50	−95

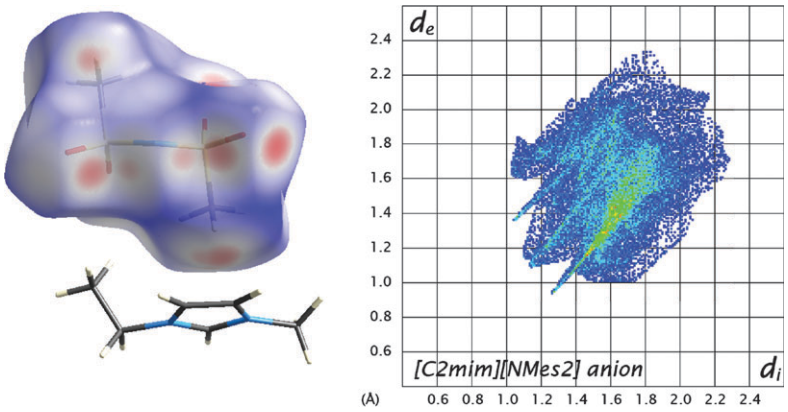

Fig. 1 Hirshfeld surface and associated fingerprint plot of the anion for $[C_2mim][NMes_2]$. The close contacts in the Hirshfeld surface appear in red [d_{norm} range: −0.38, 1.1].

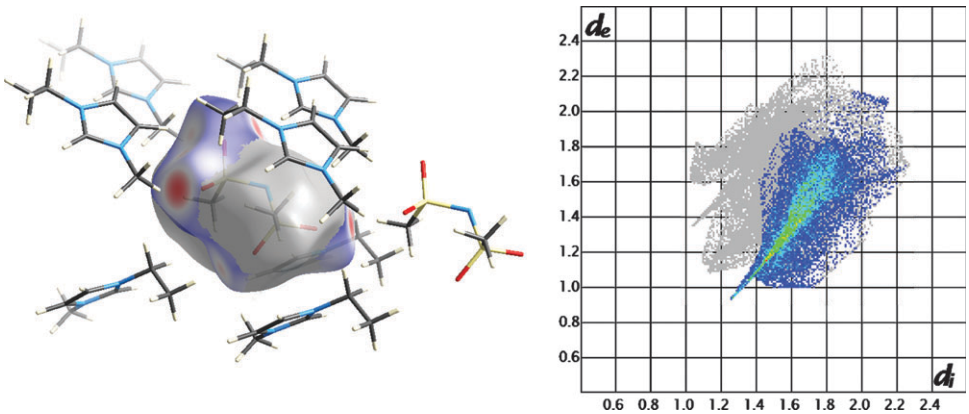

Fig. 2 Decomposed Hirshfeld surface and associated fingerprint plot of the anion for $[C_2mim][NMes_2]$ showing C–H···O hydrogen bonds. Only the molecules involved in C–H···O hydrogen bonds are shown, all molecules shown are within a 3.0 Å range of the surface. The diagonal line shown on the fingerprint plot represents those combinations of d_i and d_e that sum to the van der Waals radii. Contacts (regions of the plot) to the left of this line can be considered to be "close-contacts". [d_{norm} range: −0.38, 1.1].

Table 2 Relative percentage contributions of selected cation–anion contacts to the $NMes_2$ and NTf_2 anion (relative to the whole of the Hirshfeld surface area[a])

	$[C_1mpyr]$		$[C_4mpyr]$		$[C_2mim]$		
	$NMes_2$	NTf_2	$NMes_2$	NTf_2	$NMes_2$	NTf_2[b]	NTf_2[b]
C–H···O	43.1	33.9	44.7	37.7	41.9	34.1	35.4
C–H···N	6.1	3.7	6.0	4.0	6.5	3.8	3.9
C–H···F	—	33.4	—	48.0	—	31.8	30.7
C···H–C	—	—	—	—	4.2	—	—
C···F–C	—	—	—	—	—	2.4	2.3

[a] See ESI† for full details of fingerprint plots. [b] The relative percentage contributions of both crystallographically distinct NTf_2 anions are included, in the order N5/N6 (where N indicates the central nitrogen according to the labels used).

Table 3 Relative percentage contributions of selected anion–anion contacts to the $NMes_2$ and NTf_2 anion (relative to the whole Hirshfeld surface area[a])

	$[C_1mpyr]$		$[C_4mpyr]$		$[C_2mim]$		
	$NMes_2$	NTf_2	$NMes_2$	NTf_2	$NMes_2$	NTf_2[b]	NTf_2[b]
C–H···O	7.1	—	4.9	—	3.1	—	—
C–F···F	—	21.8	—	9.2	—	19.2	19.7

[a] See ESI† for full details of fingerprint plots. [b] The relative percentage contributions of both crystallographically distinct NTf_2 anions are included, in the order N5/N6 (where N indicates the central nitrogen according to the labels used).

a higher percentage contribution of these in both the [C_1mpyr] salts. However, the main contributors, apart from the obvious C–H···H close contacts, are the cation–anion C–H···O and C–H···F weak, non-classical, hydrogen bonds. It is interesting to note the presence of some energetically unfavourable[19] C–F···π interactions in the imidazolium case.

Detailed fingerprint plot analysis: general trends

It is immediately apparent from a comparison of the anionic plots shown in Fig. 3 that the NTf_2 salts display a larger range in d_e than the $NMes_2$ salts and *vice versa* in d_i, as a result of the larger fluorine atoms *cf.* hydrogen. The greater range of d_e indicates the less compact packing of the NTf_2 salts. However, it is evident that the plots display a greater spread of points in d_i going from [C_1mpyr] to [C_4mpyr], which is suggestive of the more compact, symmetrical [C_1mpyr] producing more dense packing than the longer chain analogues are capable of. In the region (d_i + d_e) > 2.2 Å the plots become quite scattered, indicating a number of points on the surface having separations distinctly greater than the sum of the van der Waals radii (as indicated by the diagonal lines on the plots in the ESI†); for example as seen in the C–H···H and C–F···F contacts. Noticeable within the [C_4mpyr] salts is a larger number of particularly long contacts >4 Å; such long contacts are evidence of 'voids' in the structure and non-optimum packing,[17] probably due to the bulky alkyl chains. C_4 alkyl chains are perhaps too long to encourage compact packing and too short to encourage alkyl chain intercalation. The mean value of d_{norm}, over the whole of the Hirshfeld surface, has also been calculated for each of the Hirshfeld surfaces (see Table 5 in the ESI†). This average can be thought of as a measure of packing efficiency and therefore also of relative free volume in the structure. This provides a useful connection between the structure and the transport properties and glass transition temperature since these are thought in some models[20] to be dependent on free volume. This quantity is much smaller for the [C_1mpyr] salts than their larger cation relatives, as would be expected for this more compact, more easily packed cation. It is also much smaller for the [$NMes_2$] salts than the [NTf_2] salts, thus leading one to expect that the T_g and other transport properties of the $NMes_2$ salts should be uniformly higher than the NTf_2 salts; this is as observed in Table 1. However, this approach has obvious limitations related to the fact that the free volume of the liquid state is unquestionably different to that of the crystal. Nonetheless the d_{norm} parameter provides a useful means of analysing relative free volume in these structures.

Anion–cation contacts

The 'wing' seen in the [C_2mim][$NMes_2$] plot (Fig. 3(e)) is a result of C–H···C interactions, which account for the anion methyl group hydrogens and the imidazolium π orbitals. The same is seen in the [C_2mim][NTf_2] (Fig. 3(f) and g) salts with a 'shoulder' indicating the regions of the plot arising from the C–F···π interaction at d_i ~1.5 Å. In the case of the [C_2mim][NTf_2] salt, the S–O···H and C–F···H interactions are the most prevalent, with a strong 'spike' (which is an overlap of the two interactions) in the plot, arising from close contacts around d_i: ~1.3 Å, d_e: ~1.0 Å. Overall, the NTf_2 salts, in comparison to the $NMes_2$ salts, display a more distinct 'spike' arising from a localised, close S–O···H contact. In the case of [C_1mpyr][NTf_2] (Fig. 3(b)) and [C_2mim][NTf_2] (Fig. 3(f) and (g)) this contact is very close (d_i: ~1.25 Å, d_e: ~0.85 Å). Consulting the Hirshfeld surface reveals that in these two cases the hydrogen involved in this interaction is from the ring, alpha to the nitrogen, whilst in [C_4mpyr] the hydrogen involved is from the alkyl chain. This partly explains why [C_1mpyr][NTf_2] displays strong crystalline

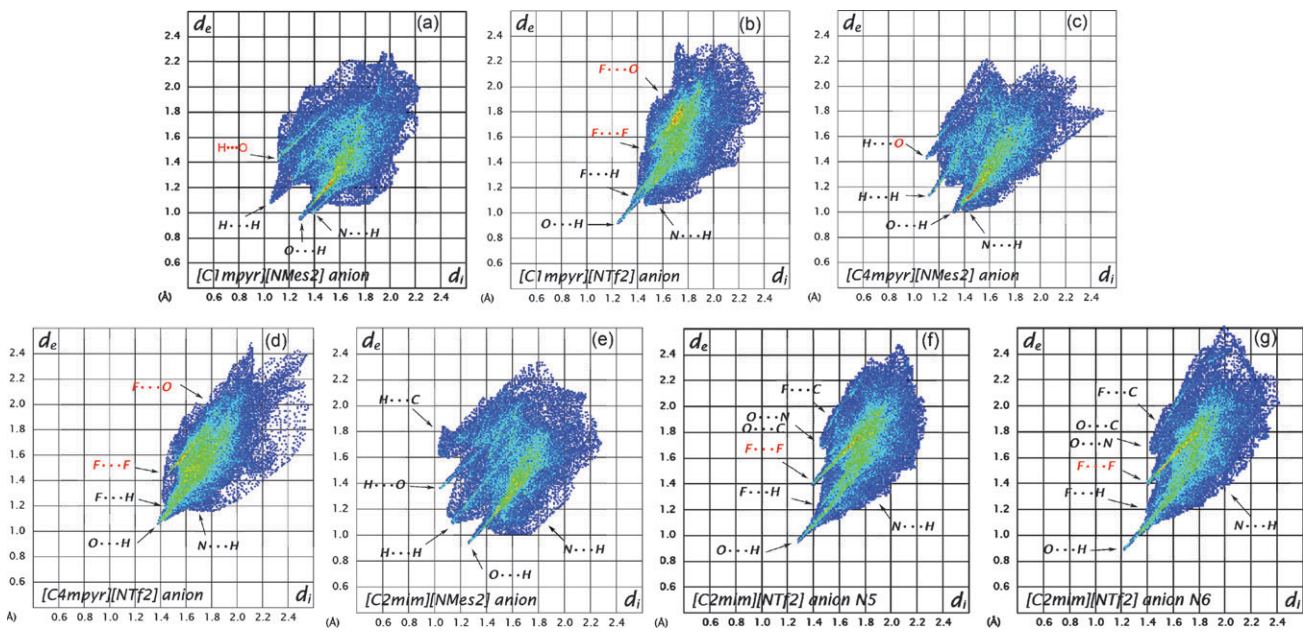

Fig. 3 Full fingerprint plots of the anions for the $NMes_2$ and NTf_2 salts. Black labels indicate regions of the plot arising from selected anion–cation contacts; red labels indicate regions of the plot arising from selected anion–anion contacts. Note: H···H contacts are both cation–anion and anion–anion in the $NMes_2$ salts.

stability (*i.e.*, higher melting point) compared to that of [C_4mpyr][NTf_2],. The cation C–H···N (amide) interaction is situated to the bottom right (overall bond length 2.4–2.5 Å) of each plot and is interspersed amongst the C–H···H interactions.

Anion–anion contacts

In addition to the cation–anion contacts discussed above, [C_2mim][NTf_2] (Fig. 3(f) and (g)) also displays very prominent C–F···F interactions, indicated by the short spike at d_i: ~1.4 Å, d_e: ~1.4 Å. It is also interesting to note that some of the F–F distances are shorter than the sum of the van der Waals radii, despite the fact that these interactions are normally weak.[19] This may be a reflection of the overall stabilisation of the lattice, in particular the Madelung energy of the lattice arising from its ionic nature. Presumably the overall cohesive binding energy of the lattice dominates. The anion–anion C–H···O interaction in the $NMes_2$ salts are also clearly seen as the spike arising from the close contact at (d_i: ~1.1 Å, d_e: ~1.4 Å). The remaining spike/protrusion in the $NMes_2$ series is due to the C–H···H interactions, as is clearly seen in Fig. 3(a) and (c), which make up a larger fraction of the Hirshfeld surface than in the NTf_2 salts, probably due to the inter-anionic interactions in this case. Overall these observations seem to indicate stronger H-bonded anion–anion interactions in the $NMes_2$ case, in accord with their typically higher T_g and viscosity in the liquid state.

Conclusion

This paper highlights the usefulness of the Hirshfeld analysis in understanding the intricacies of interactions occurring in crystallised ionic liquids. The presence of C–F···π and C–H···π interactions were identified and the importance of anion–anion interactions also becomes clear. Overall, the dominant interaction in all of the structures was found to be the C–H···O close contact, thus agreeing with past literature. However, the Hirshfeld surface and its associated fingerprint plot certainly allows a much more detailed scrutiny and comparison of related structures. Thus, prepared with the full knowledge of all of the interactions occurring in crystallised ILs one is better able to understand the dominant features and potentially to better design new ionic liquids with desired physical properties.

Methods

Hirshfeld surface analysis

The program CrystalExplorer 2.0 was used to render all surfaces and fingerprint plots. Previously published crystal structures used for this study: [C_1mpyr][$NMes_2$], CSD refcode ULOJOU; [C_1mpyr][NTf_2], CSD refcode XOMDIM; [C_2mim][NTf_2], CSD refcode RENSEJ and [C_4mpyr][NTf_2], CSD refcode LAZREK.

DSC experiments

DSC experiments were performed on a T.A. Instruments Perkin-Elmer Q100. Samples of mass 5–20 mg were sealed in a vented aluminium pan and placed in the furnace with a 50 ml min^{-1} nitrogen stream; the temperature was raised at 10 °C min^{-1}. The reference was an empty aluminium pan.

Crystallography

Crystallisation of [C_4mpyr][$NMes_2$] and [C_2mim][$NMes_2$] was observed in the neat ionic liquids after careful storage of the original samples for >2 years. The reflection intensity data were measured on a Bruker X8 APEX KAPPA CCD Single Crystal X-ray Diffractometer, using graphite-monochromated Mo-Kα radiation (λ = 0.71073 Å). Crystals were coated with Paratone N oil (Exxon Chemical Co., TX, USA) immediately after isolation and cooled in a stream of nitrogen vapour on the diffractometer. Structures were solved by direct methods using the program SHELXS-97[21] and refined using SHELXL-97.[21] All non-hydrogen atoms were revealed in the E-map and subsequent difference electron density maps and thus placed and refined anisotropically. All H atoms were observed in difference syntheses and were placed in geometrically idealised positions and constrained to ride on their parent atoms with C···H distances in the range 0.95–1.00 Å and $U_{iso}(H) = xU_{eq}(C)$, where x = 1.5 for methyl and 1.2 for all other C atoms.

Crystal data for [C_2mim][$NMes_2$]. $C_6H_{11}N_2{\cdot}C_2H_6N_1O_4S_2$, M = 283.37, monoclinic, space group $P2_1$, a = 6.2135(2), b = 13.7443(4), c = 7.8355(2) Å, β = 106.172(2)°, U = 642.67(3) $Å^3$, Z = 2, D_c = 1.464, T = 123(2) K, μ(Mo-Kα) = 0.422 mm^{-1}. Full-matrix least-squared refinement was based on 2931 reflection data and yielded $wR2$ = 0.0620 (all data), $R1$ [2931 data with $F^2 > 2\sigma(F^2)$] = 0.0248, and goodness-of-fit on F^2 = 1.099.

Crystal data for [C_4mpyr][$NMes_2$]. $C_9H_{20}N_1{\cdot}C_2H_6N_1O_4S_2$, M = 314.46, orthorhombic, space group $Pbca$, a = 13.7961(7), b = 10.955(6), c = 20.8776(10) Å, U = 3155.4 (20) $Å^3$, Z = 8, D_c = 1.324, T = 123(2) K, μ(Mo-Kα) = 0.349 mm^{-1}. Full-matrix least-squared refinement was based on 3621 reflection data and yielded $wR2$ = 0.1000 (all data), $R1$ [3289 data with $F^2 > 2\sigma(F^2)$] = 0.0407, and goodness-of-fit on F^2 = 1.136.

Acknowledgements

P. M. D. is grateful to Monash University for the Monash Graduate Scholarship and Monash International Post-graduate Research Scholarship, J. M. P. and D. R. M. are grateful to the Australian Research Council for a QEII Fellowship and Federation Fellowship, respectively.

References

1 V. Landnak, N. Hofmann, N. Brausch and P. Wasserscheid, *Adv. Synth. Catal.*, 2007, **349**, 719.
2 M. Haumann, K. Dentler, J. Joni, A. Riisager and P. Wasserscheid, *Adv. Synth. Catal.*, 2007, **349**, 425.
3 C. F. Poole, *Adv. Chromatogr.*, 2007, **45**, 89.
4 (*a*) P. C. Howlett, N. Brack, A. F. Hollenkamp, M. Forsyth and D. R. MacFarlane, *J. Electrochem. Soc.*, 2006, **153**, A595; (*b*) W. Lu, A. G. Fadeev, B. H. Qi, E. Smela, B. R. Mattes, J. Ding, G. M. Spinks, J. Mazurkiewicz, D. Z. Zhou, G. G. Wallace, D. R. MacFarlane, S. A. Forsyth and

M. Forsyth, *Science*, 2002, **297**, 983; (*c*) D. R. Macfarlane, M. Forsyth, P. C. Howlett, J. M. Pringle, J. Sun, G. Annat, W. Neil and E. I. Izgorodina, *Acc. Chem. Res*., 2007, **40**, 1165.
5 W. L. Hough, M. Smiglak, H. Rodriguez, R. P. Swatloski, S. K. Spear, D. T. Daly, J. Pernak, J. E. Grisel, R. D. Carliss, M. D. Soutullo, J. H. Davis, Jr and R. D. Rogers, *New J. Chem*., 2007, **31**, 1429.
6 V. R. Koch, C. Nanjundiah, G. Battista Appetecchi and B. Scrosati, *J. Electrochem. Soc*., 1995, **142**, L116.
7 P. Bonhote, A. Dias, N. Papageorgiou, K. Kalyanasundaram and M. Gratzel, *Inorg. Chem*., 1996, **35**, 1168.
8 L. A. Dominey, V. R. Koch and T. J. Blakley, *Electrochim. Acta*, 1992, **37**, 1551.
9 J. M. Pringle, J. Golding, K. Baranyai, C. M. Forsyth, G. B. Deacon, J. L. Scott and D. R. MacFarlane, *New J. Chem*., 2003, **27**, 1504.
10 C. M. Forsyth, D. R. MacFarlane, J. J. Golding, J. Huang, J. Sun and M. Forsyth, *Chem. Mater*., 2002, **14**, 2103.
11 W. A. Henderson, V. G. Young, Jr, S. Passerini, P. C. Trulove and H. C. De Long, *Chem. Mater*., 2006, **18**, 934.
12 A. R. Choudhury, N. Winterton, A. Steiner, A. I. Cooper and K. A. Johnson, *J. Am. Chem. Soc*., 2005, **127**, 16792.
13 A. R. Choudhury, N. Winterton, A. Steiner, A. I. Cooper and K. A. Johnson, *CrystEngComm*, 2006, **8**, 742.
14 J. D. Holbrey, W. M. Reichert and R. D. Rogers, *Dalton Trans*., 2004, 2267.
15 J. J McKinnon, A. S. Mitchell and M. A. Spackman, *Chem.–Eur. J*., 1998, **4**, 2136.
16 J. J. McKinnon, M. A. Spackman and A. S. Mitchell, *Acta Crystallogr., Sect. B: Struct. Sci*., 2004, **60**, 627.
17 M. A. Spackman and J. J. McKinnon, *CrystEngComm*, 2006, **4**, 378.
18 J. J. McKinnon, D. Jayatilaka and M. A. Spackman, *Chem. Commun*., 2007, 3814.
19 K. Reichenbacher, H. I. Suss and J. Hulliger, *Chem.Soc. Rev*., 2005, **34**, 22.
20 S. I. Smedley, in *The Interpretation of Ionic Conductivity in Liquids*, Plenum Press, New York, 1980, ch. 3, pp. 82–83.
21 G. M. Sheldrick, *Acta Crystallogr., Sect. A: Found. Crystallogr*., 2008, **64**, 112.

